Supporting Information

Regular Article

Tuning chemical properties on ruthenium(II) complexes through PEGylation of N-heterocyclic carbene ligands

Oscar Barrios[1,2], Tamara Rodriguez-Prieto[1], Alicia Bort,[3] Elżbieta Okła,[4] Marek Maly[5], Miriam Chavez-Peraza[6], Alberto Escarpa[6], Maksim Ionov,[4,7] Maria Bryszewska,[4] Jesús Cano[1,2,8], Inés Díaz-Laviada[3]*, Rafael Gómez[1,2,8]*

[1] University of Alcalá, Department of Organic and Inorganic Chemistry and Research Institute in Chemistry "Andrés M. Del Río" (IQAR), Madrid, Spain.
[2] Networking Research Center on Bioengineering, Biomaterials and Nanomedicine (CIBER-BBN), Madrid, Spain.
[3] University of Alcalá, Biochemistry and Molecular Biology Unit. Department of Systems Biology and and Research Institute in Chemistry "Andrés M. Del Río" (IQAR), Madrid, Spain.
[4] Faculty of Biology and Environmental Protection, Department of General Biophysics, University of Lodz, Pomorska 141/143, Lodz 90–236, Poland.
[5] Department of Physics, Faculty of Science, University of Jan Evangelista Purkyně in Ústí nad Labem, Pasteurova 15, 400 96 Ústí nad Labem, Czech Republic
[6] University of Alcalá, Department of Analytical Physical-Chemistry and Chemical Engineering and Research Institute in Chemistry "Andrés M. Del Río" (IQAR), Madrid, Spain
[7] Collegium Medicum, Faculty of Medicine, Mazovian Academy in Plock, Pl. Dabrowskiego 2, Plock 09-402, Poland.
[8] Ramón y Cajal Health Research Institute (IRYCIS), IRYCIS, Madrid 28034, Spain.

*Corresponding author: rafael.gomez@uah.es; Tel: (+34) 91 8854685; ines.diazlaviada@uah.es; Tel: (+34) 91 8855141

Received: date; Accepted: date; Published: date

INDEX

S1. Synthetic protocols of ligands L3-L8.

General procedure for the synthesis of the corresponding MeO-PEGMw-OMs.

For the formation of the corresponding mesylated-PEG derivatives, a mixture of n-ethyleneglycol monomethylether (MeO-PEG_{Mw}-OH) and pirydine (2equiv.) was prepared under argon. Methanesulfonylchloride (2 equiv.) was added drop by drop with a dropping funnel to the mixture previously cooled. Then, the mixture was let to temper and stirred overnight. The following day, the mixture was extracted by a saturated $NaHSO_3$ solution so that the remaining pyridine is removed as a cationic species. Afterwards, organic phase was again extracted by a previously calibrated pH=7-8 sodium hydroxide solution, to ensure the withdrawal of the methanesulfonyl chloride excess as hydroxide derivative. Finally, the organic phase was dried with NaSO4, filtered and dried under vacuum.

Synthesis of (MeO-PEG_{500})-OMs (L3). Compound **L3** was synthesised following the general procedure previously described. Polyethyleneglycol monomethylethylether (Mw=550) (4.03 ml, 7.96 mmol, 1 equiv.); pyridine (1.3 ml, 15.9 mmol, 2 equiv.); methanesulfonyl chloride (1.2 ml, 15.9 mmol, 2 equiv); compound **L3** afforded (4.68 g, 93.6% yield). ^{1}H NMR (400 MHz, $CDCl_3$): δ 4.35 (m, 2H, CH_2 PEG500), 3.73 (m, 2H, $CH_{2\ PEG500}$), 3.61 (m, $(CH_{2\ PEG500})_n$), 3.52 (m, 2H, $CH_{2\ PEG500}$), 3.34 (s, 3H, $CH_{3\ OMe\ PEG500}$), 3.05 (s, 3H, $CH_{3\ OMs\ PEG500}$) ppm. ^{13}C NMR (101 MHz, $CDCl_3$): δ 71.85 ($CH_{2\ PEG500}$), 70.48 ($(CH_{2\ PEG500})_n$), 69.31 ($CH_{2\ PEG\ 500}$), 68.94 ($CH_{2\ PEG500}$), 58.94 ($CH_{3\ OMe}$), 37.65 ($CH3_{\ OMs}$). $[M+H]^+$= 639.33 Da (polydispersity can be observed in the mass spectra, see Figure S1).

Synthesis of (MeO-PEG_{2000})-OMs (L4). Compound **L4** was synthesised following the general procedure previously described. Polyethyleneglycol monomethylethylether (Mw=2000) (9.6 g, 4.8 mmol, 1 equiv.); pyridine (0.8 ml, 9.6 mmol, 2 equiv); methanesulfonyl chloride (0.7 ml, 9.62 mmol, 2 equiv); compound **L4** afforded (7.7 g, 77% yield). ^{1}H NMR (400 MHz, $CDCl_3$): δ 4.37 (m, 2H, $CH_{2\ PEG2000}$), 3.63 (m, $(CH_{2\ PEG2000})_n$), 3.37 (s, 3H, $CH_{3\ OMe\ PEG2000}$), 3.07 (s, 3H, $CH_{3\ OMs\ PEG2000}$) ppm. ^{13}C NMR (101 MHz, $CDCl_3$): δ 71.28 ($CH_{2\ PEG2000}$), 69.78 ($(CH_{2\ PEG2000})_n$), 68.76 ($CH_{2\ PEG2000}$), 68.33 ($CH_{2\ PEG2000}$), 58.27 ($CH_{3\ OMe\ PEG2000}$), 36.96 ($CH_{3\ OMs\ PEG2000}$) ppm.

General procedure for the synthesis of the 1-PEG_{Mw}-4,5-dichloroimidazole derivatives

First, sodium hydride-60 % dispersion in mineral oil was washed three times with hexane under argon and the final solid was dried under vacuum to remove possible hexane traces. Following, the solid was dissolved in dry THF and cooled in an ice bath. Once cooled, 4,5-dichloroimidazole was added to the solution and let to stir for one hour. Afterwards, the slight overpressure generated by the hydrogen formation was released by vacuum. Then, the corresponding mesylated PEG species was added drop by drop to the mixture under argon. The final mixture was heated at 66 ºC and let to stir overnight. The following day, purification was carried out. First, the mixture was filtered to remove sodium salts and sodium hydride excess. The filtrate was dried and dissolved in DCM to remove insoluble species by filtration and finally dried under vacuum affording the desired product.

Synthesis of 1-PEG_{500}-4,5-dichloroimidazole (L5). Compound **L5** was synthesised following the general procedure previously described. Sodium hydride-60% dispersion in mineral oil (54 mg, 0.9 mmol, 3 equiv.); 4,5-dichloroimidazole (1 g, 7.4 mmol, 1 equiv.); compound L3 (4.7 g, 7.4 mmol, 1 equiv); compound **L5** afforded (4.0 g, 80.6%). ^{1}H NMR (400 MHz, $CDCl_3$): δ 7.45 (s, 1H, $CH_{Imid\text{-}2'}$), 4.01 (t, J = 5.1 Hz, 2H, $CH_{2\ PEG500}$), 3.68 – 3.44 (m, $(CH_{2\ PEG500})_n$), 3.31 (s, 3H, $CH_{3\ OMe\ PEG500}$) ppm. ^{13}C NMR (101 MHz, $CDCl_3$) δ 135.76 ($C_{Imid\text{-}2'}$), 72.13 ($CH_{2\ PEG500}$), 70.76 (($CH_{2\ PEG500})_n$), 69.13 ($CH_{2\ PEG500}$), 59.23 ($CH_{3\ Me\text{-}Imid}$), 46.22 ($CH_{2\ PEG500}$) ppm.

Synthesis of 1-PEG_{2000}-4,5-dichloroimidazole (L6). Compound **L6** was synthesised following the general procedure previously described. Sodium hydride-60% dispersion in mineral oil (420 mg, 2.3 mmol, 3 equiv.); 4,5-dichloroimidazole (320 mg, 2.3 mmol, 1 equiv.); compound L3 (4.90 g, 2.3 mmol, 1 equiv); compound **L6** afforded (3.52 g, 70.4 %). ^{1}H NMR (400 MHz, $CDCl_3$): δ 7.51 (s, 1H, $CH_{Imid\text{-}2'}$), 4.08 (t, J = 5.1 Hz, 2H, $CH_{2\ PEG2000}$), 3.64 (m, $(CH_{2\ PEG2000})_n$), 3.38 (s, 3H, $CH_{3\ OMe\ PEG2000}$).^{13}C NMR (101 MHz, $CDCl_3$) δ 135.76 ($C_{Imid\text{-}2'}$), 72.13 ($CH_{2\ PEG2000}$), 70.76 (($CH_{2\ PEG\ 2000})_n$), 69.13 ($CH_{2\ PEG2000}$), 59.23 ($CH_{3\ Me\text{-}Imid}$), 46.22 ($CH_{2\ PEG2000}$) ppm. ^{13}C NMR (101 MHz, $CDCl_3$): δ 135.76 ($C_{Imid\text{-}2'}$), 72.12 ($CH_{2\ PEG2000}$), 70.74 ($CH_{2\ PEG2000}$), 69.12 ($CH_{3\ Me\text{-}Imid}$), 46.21 ($CH_{2\ PEG2000}$) ppm.

General procedure for the synthesis of the 1-PEG$_{Mw}$-3-Methyl-4,5-dichloroimidazolium chloride derivatives.

The formation of the imidazolium derivatives was driven by the methylation with iodomethane. First, reagents were dissolved in dry acetonitrile and let to stir overnight at 100 ºC. The following day the mixture was evaporated to dryness under vacuum to withdraw the excess of iodomethane added, affording the pure compound. Relevant shift of the acidic proton of the imidazole ring was observable, confirming the imidazolium salt formation. For completion of the synthesis, the afforded compound was dissolved in water and let to stir for 48 h with amberlite chloride form so that to change the counterion. Finally, the corresponding chloride imidazolium salt was obtained.

Synthesis of 1-PEG$_{500}$-3-Me-4,5-dichloroimidazolium chloride (L7). Compound **L7** was synthesised following the aforementioned procedure. Compound **L5** (1 g, 1.5 mmol, 1 equiv.); iodomethane (0.1 ml, 4.5 mmol, 3 equiv.); compound **L7** afforded (1.28 g, 74.6% yield). ^{1}H NMR (400 MHz, $CDCl_3$): δ 11.13 (s, 1H, $CH_{Imid\text{-}2'}$), 4.58 (m, 2H, $CH_{2\ PEG500}$), 4.06 (s, 3H, CH_3 Me-Imid), 3.99 (m, 2H, $CH_{2\ PEG500}$), 4.02-3.97 (m, $(CH_{2\ PEG500})_n$), 3.37 (s, 3H, $CH_{3\ OMe\ PEG500}$) ppm. ^{13}C NMR (101 MHz, $CDCl_3$): δ 139.05 ($C_{Imid\text{-}2'}$), 72.11 ($CH_{2\ PEG500}$), 70.74 ($CH_{2\ PEG500}$), 70.69 (($CH_{2\ PEG500})_n$), 70.64 ($CH_{2\ PEG500}$), 59.21 ($CH_{3\ OMe\ PEG500}$), 48.99 ($CH_{2\ PEG500}$), 35.54 (CH_3 Me-Imid) ppm. [M]+= 605.26 u. (polydispersity can be observed in the mass spectra, see Figure S5)

Synthesis of 1-PEG$_{2000}$-3-Me-4,5-dichloroimidazolium chloride (L8). Compound **L8** was synthesised following the aforementioned procedure. Compound **L6** (640 mg, 0.3 mmol, 1 equiv.); iodomethane (60 µl, 0.9 mmol, 3 equiv.); compound **L8** afforded (359.8 mg, 54.7 % yield). ^{1}H NMR (400 MHz, $CDCl_3$): δ 11.18 (s, 1H, $CH_{Imid\text{-}2'}$), 4.59 (m, 2H, $CH_{2\ PEG2000}$), 4.06 (s, 3H, $CH_{3\ Me\text{-}Imid}$), 3.99 (m, 2H, $CH_{2\ PEG2000}$), 3.85 – 3.41 (m, $(CH_{2\ PEG2000})_n$), 3.37 (s, 3H, $CH_{3\ OMe\ PEG2000}$) ppm. ^{13}C NMR (126 MHz, $CDCl_3$): δ 139.09 ($CH_{Imid\text{-}2'}$), 72.06 ($CH_{2\ PEG2000}$), 70.73 (($CH_{2\ PEG2000})_n$), 67.71 ($CH_{2\ PEG2000}$), 59.16 ($CH_{3\ OMe}$), 48.95 ($CH_{2\ PEG2000\text{-}Imid}$), 35.50 ($CH_{3\ Me\text{-}Imid}$).

S2. Characterization data of ligands L3-L8.

A

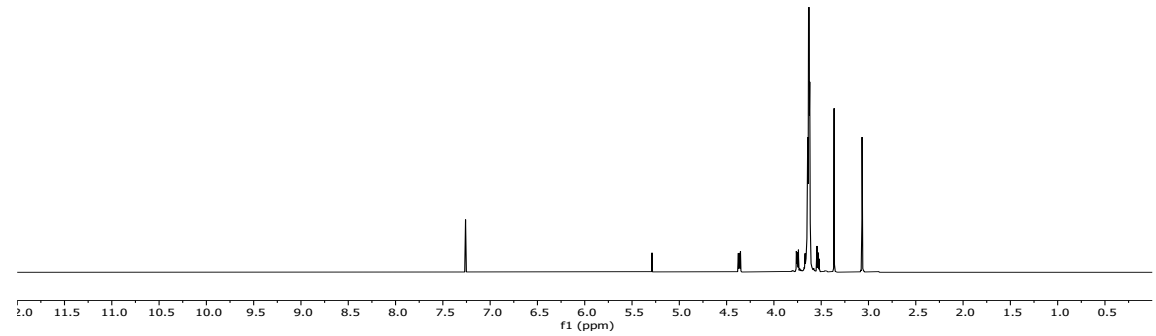

B

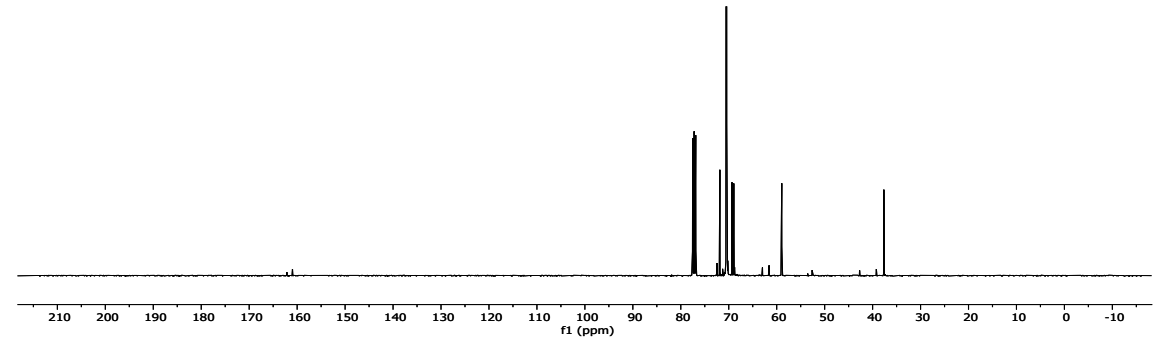

C

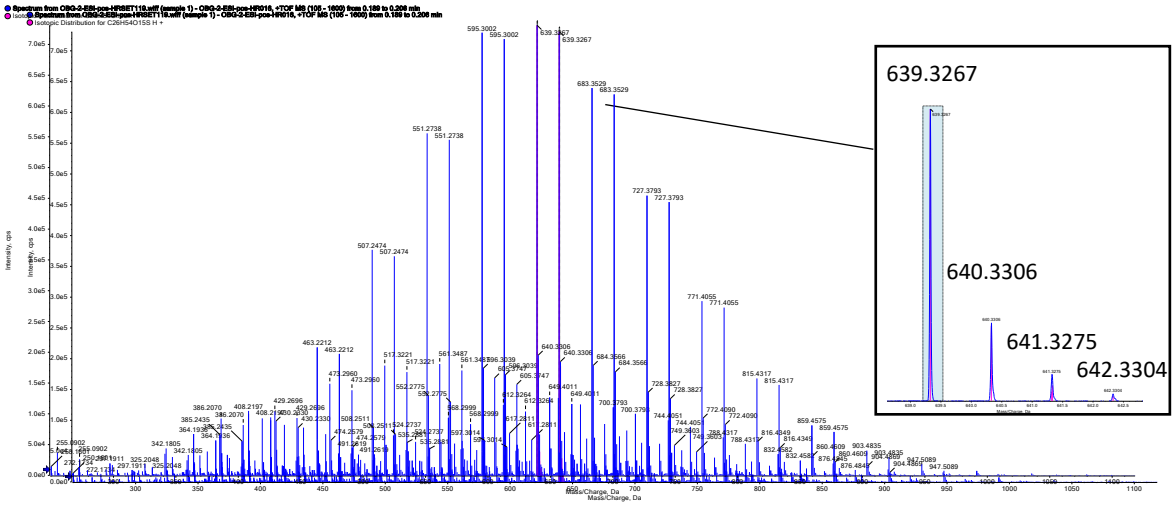

Figure S1. Characterization of compound **L3**. A) ^{1}H NMR spectrum in $CDCl_3$. B) ^{13}C NMR spectrum in CDCl3. C) Mass spectrum from ESI-TOF MS. The two more intense peaks correspond to Ms-$(CH_2CH_2O)_n$Me: n= 11, MW = 594 Da; n = 12, MW = 638 Da.

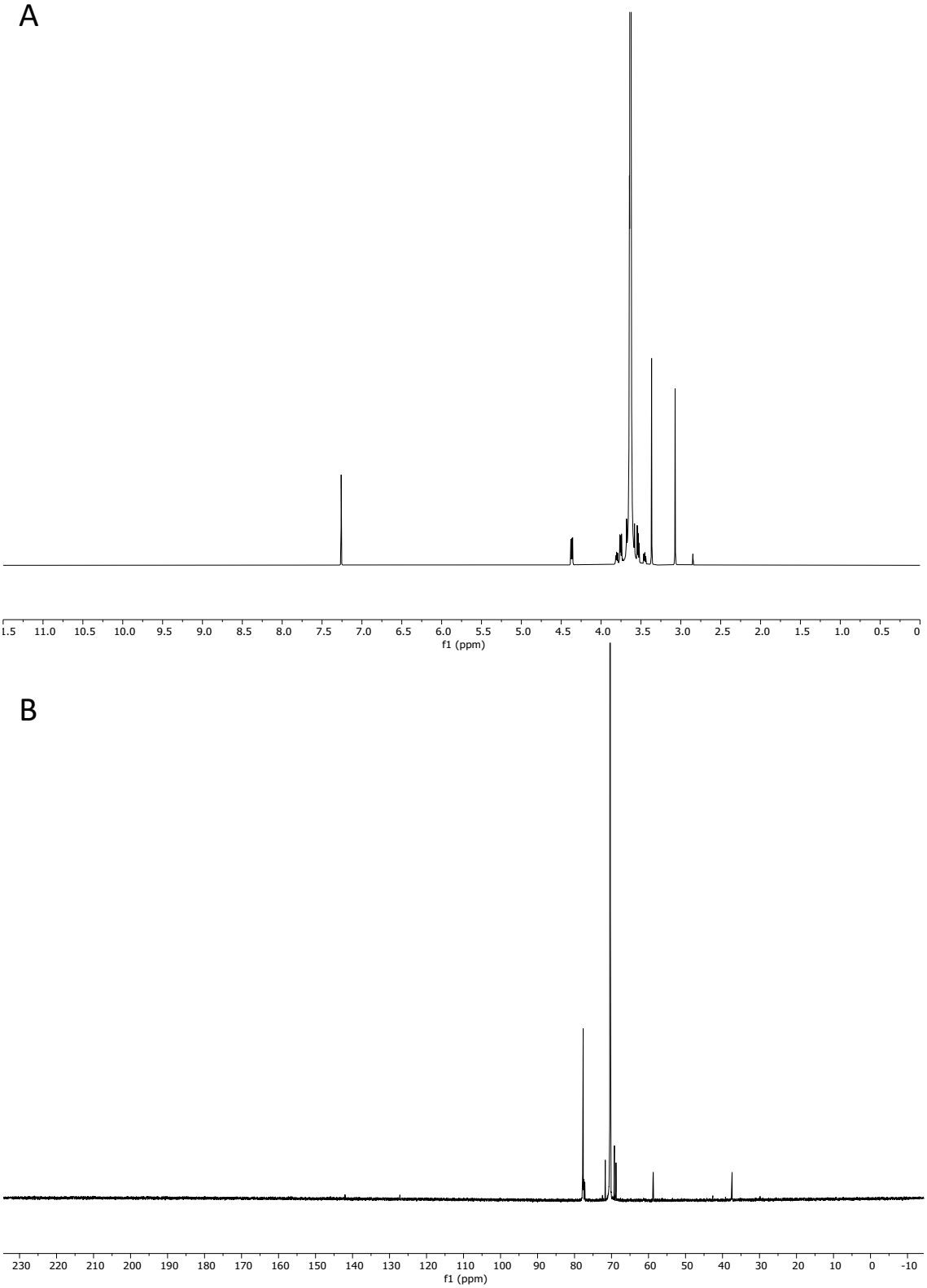

Figure S2. Characterization of compound **L4**. A) ^{1}H NMR spectrum in $CDCl_3$. B) ^{13}C NMR spectrum in $CDCl_3$.

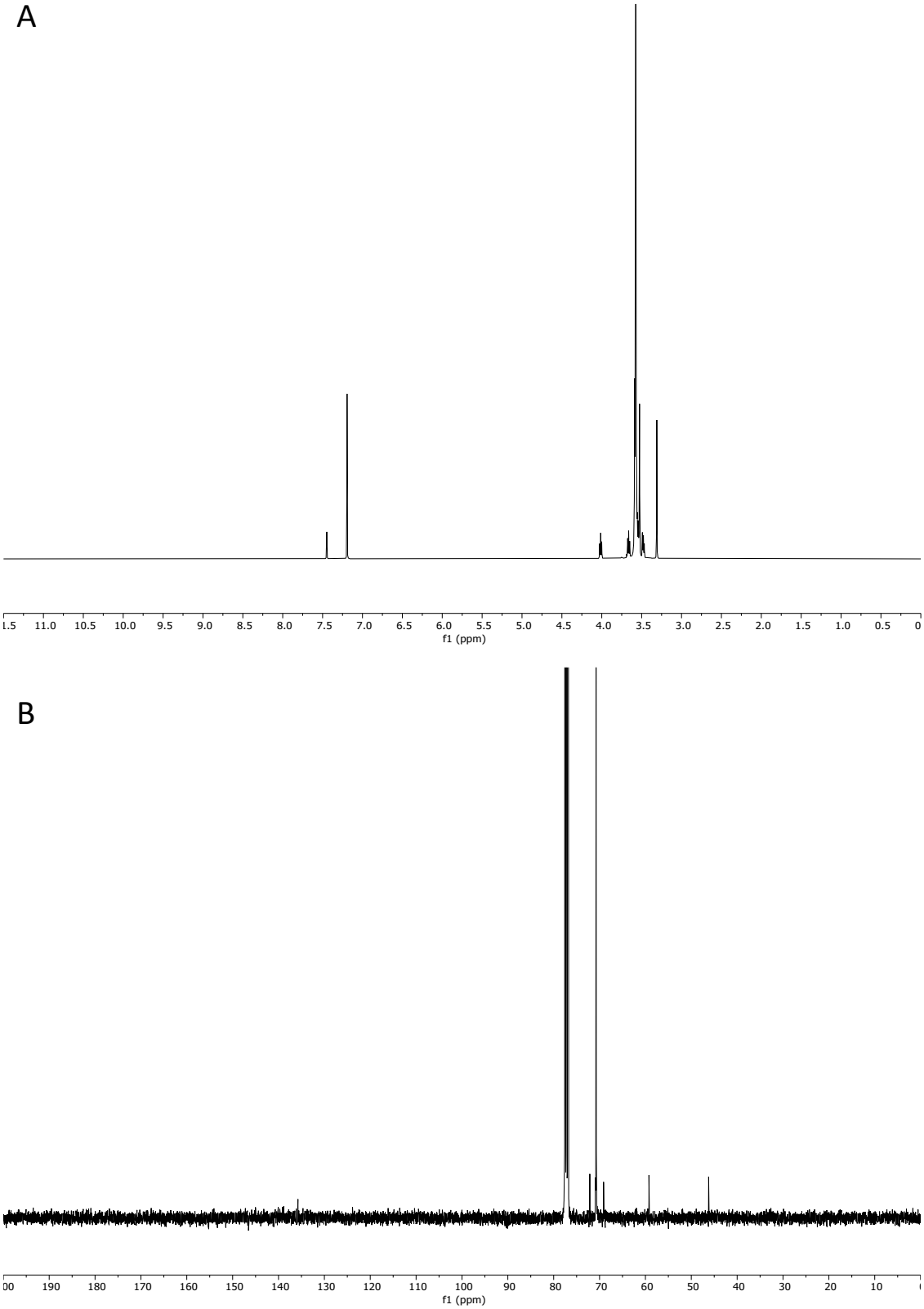

Figure S3. Characterization of compound **L5**. A) ^{1}H NMR spectrum in $CDCl_3$. B) ^{13}C NMR spectrum in $CDCl_3$.

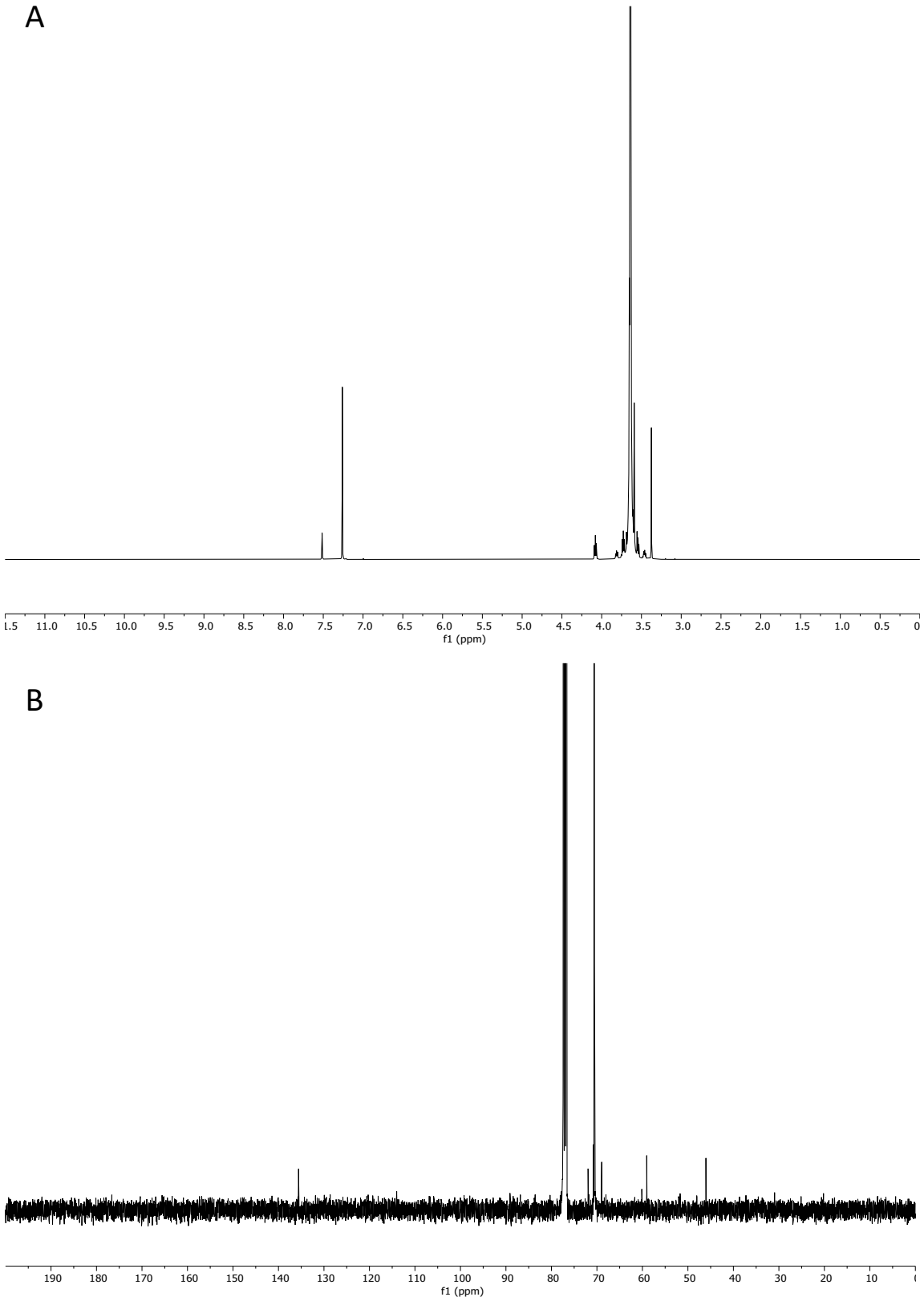

Figure S4. Characterization of compound **L6**. A) ^{1}H NMR spectrum in $CDCl_3$. B) ^{13}C NMR spectrum in $CDCl_3$.

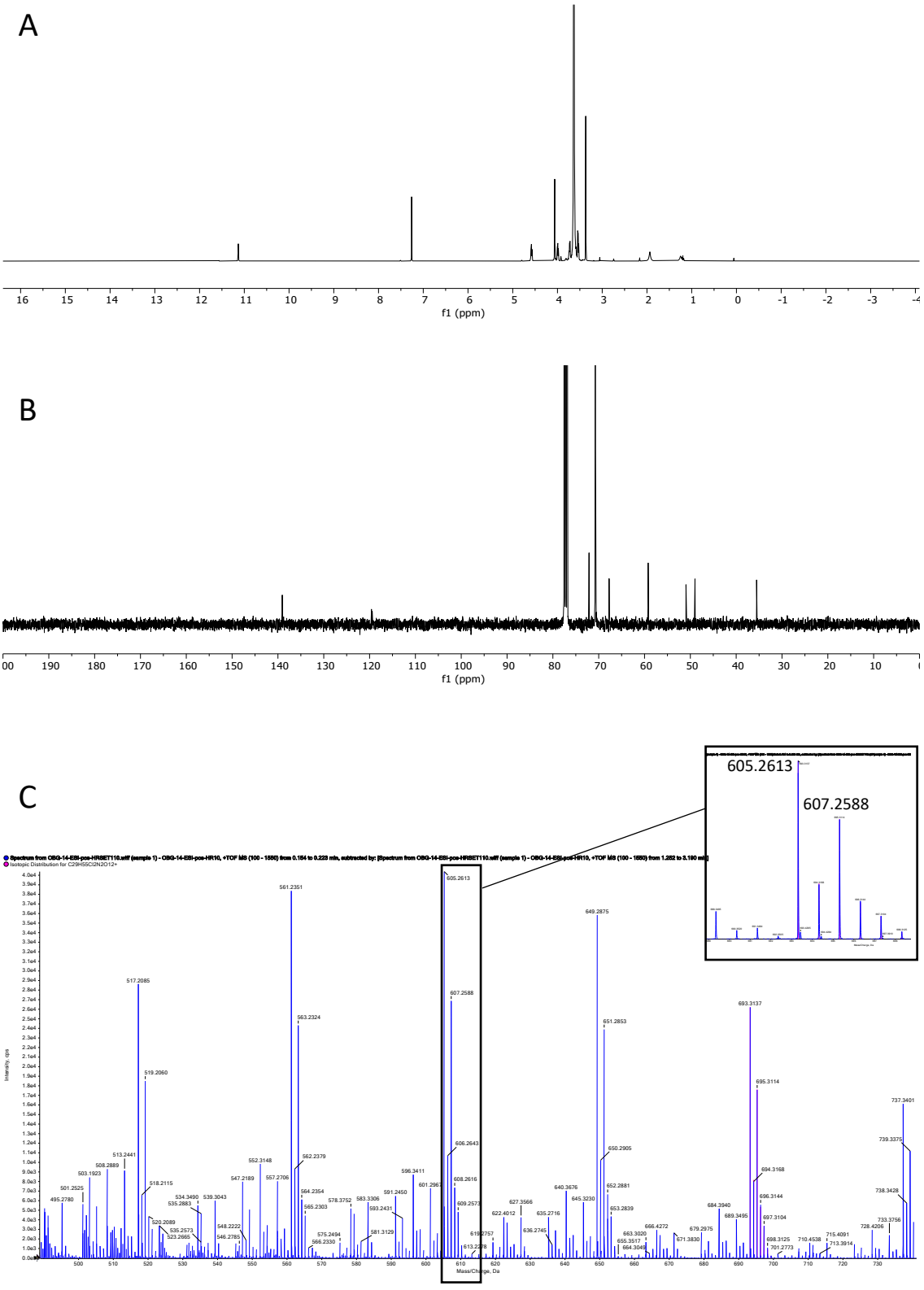

Figure S5. Characterization of compound **L7**. A) ^{1}H NMR spectrum in $CDCl_3$. B) ^{13}C NMR spectrum in $CDCl_3$. C) Mass spectrum from ESI-TOF MS. The peaks corresponding

to imidazolium-$(CH_2CH_2O)_nMe$: n= 11, MW = 650 Da; n = 12, MW = 694 Da. The more intense peak corresponds to n = 10.

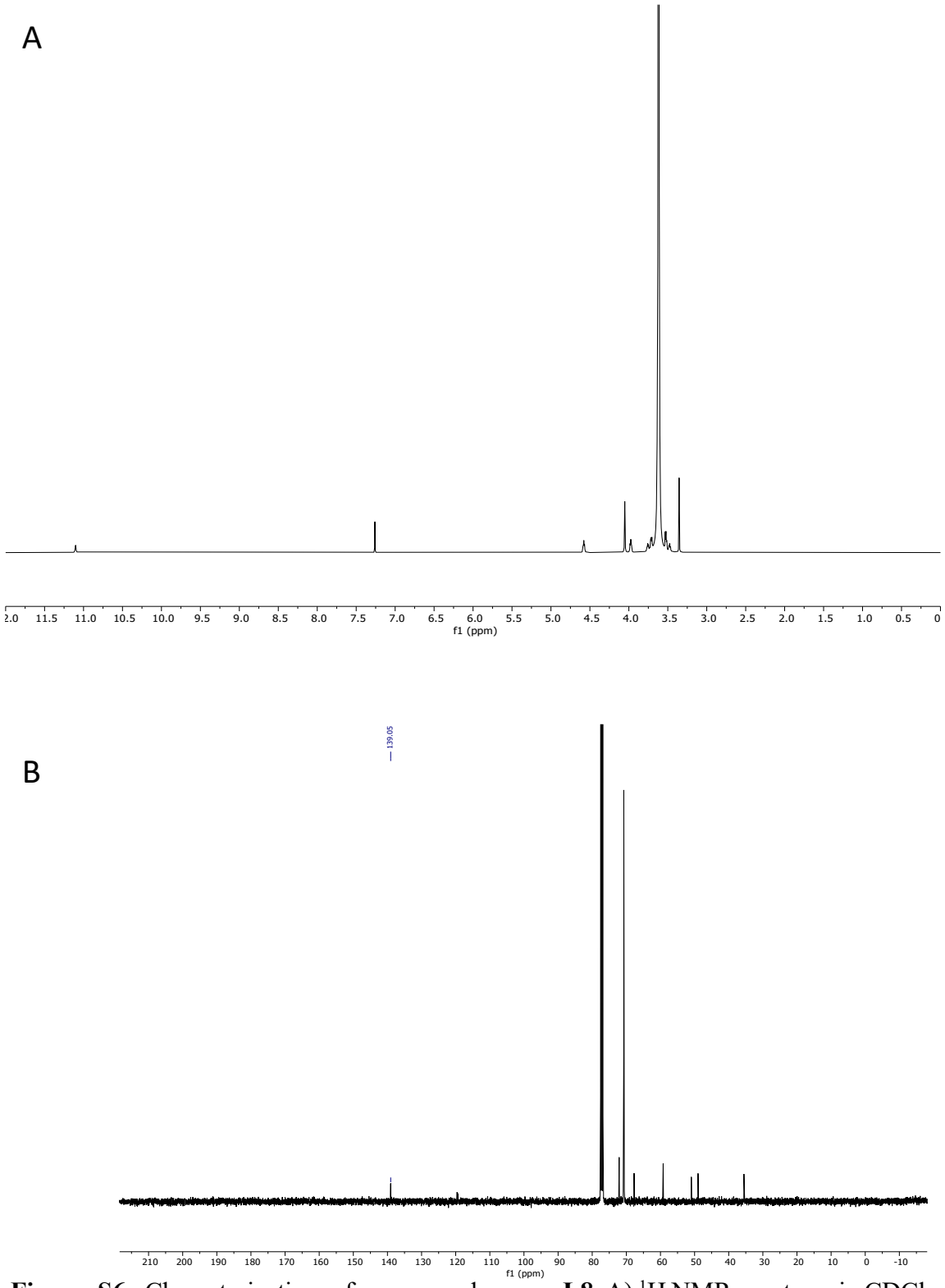

Figure S6. Characterization of compound **L8**. A) ^{1}H NMR spectrum in $CDCl_3$. B) ^{13}C NMR spectrum in $CDCl_3$.

S3. Characterization data of complexes 2 and 3.

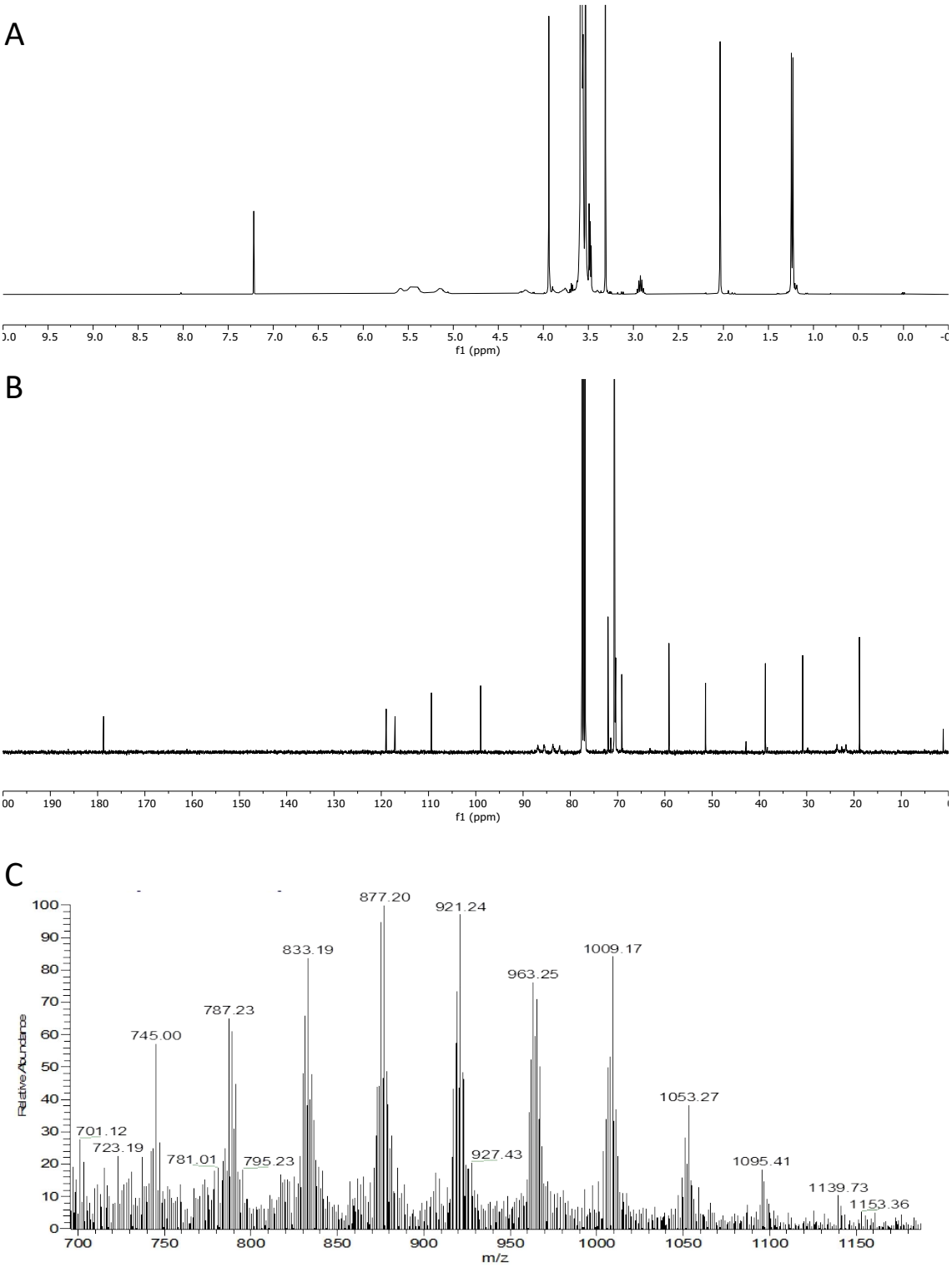

Figure S7. Characterization of complex **2**. A) ^{1}H NMR spectrum in $CDCl_3$. B) ^{13}C NMR spectrum in $CDCl_3$. C) Mass spectrum from ESI-TOF MS. The peaks corresponding to $\{[(cymene)ClRu]-(CH_2CH_2O)_nMe\}^+$: n= 11, MW = 920 Da; n = 12, MW = 963 Da. The more intense peak corresponds to n = 10 and 11.

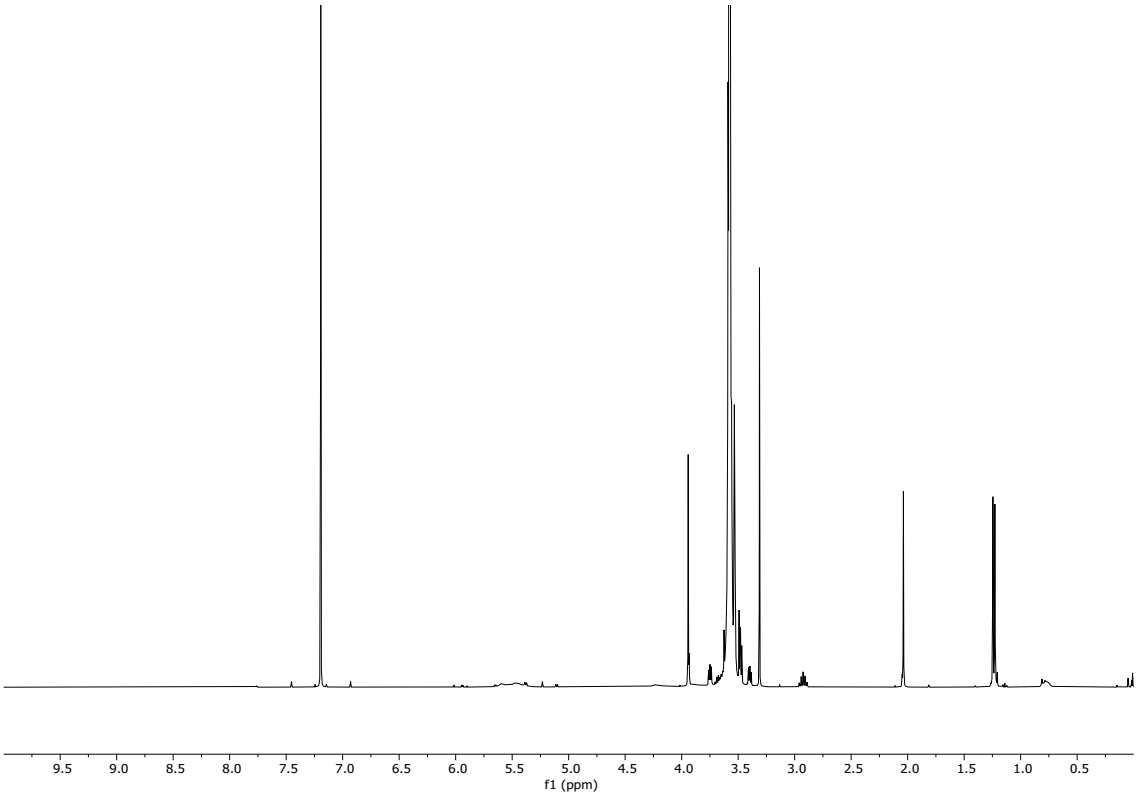

A

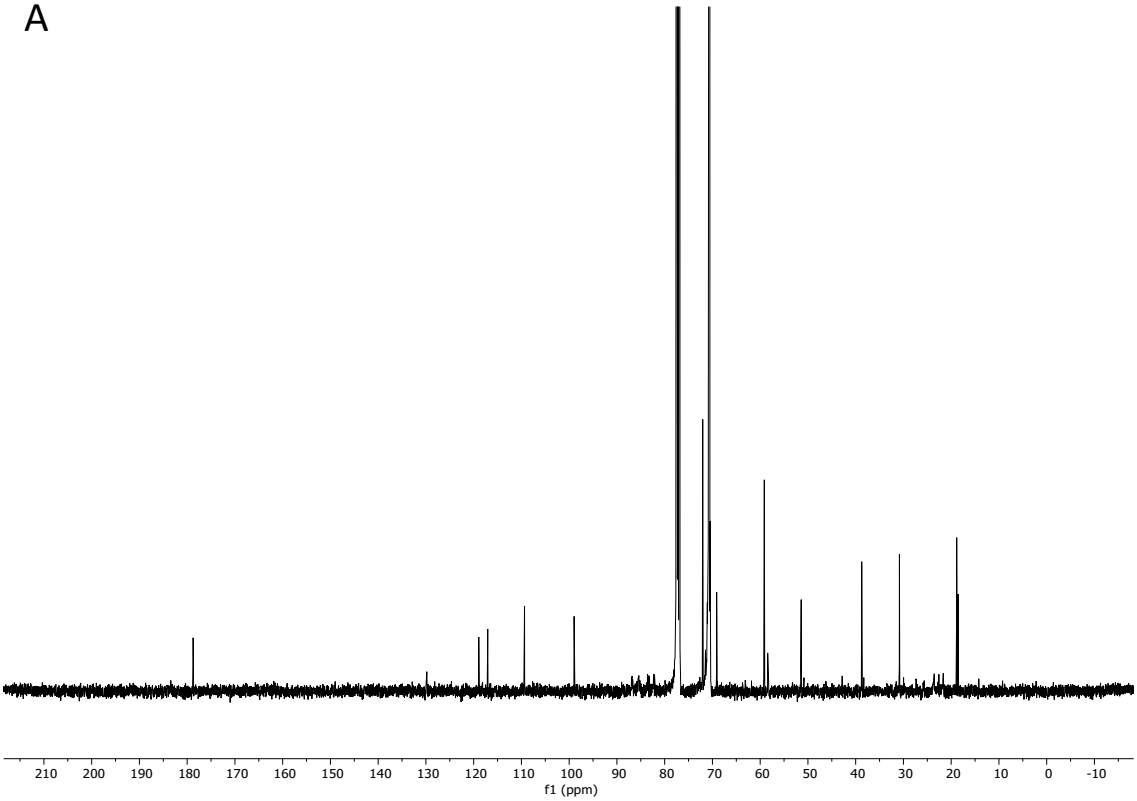

B

ure S8. Characterization of complex **3**. A) ^{1}H NMR spectrum in $CDCl_3$. B) ^{13}C NMR spectrum in $CDCl_3$.

S4.- Molecular modelling of complexes 1-3 with water molecules.

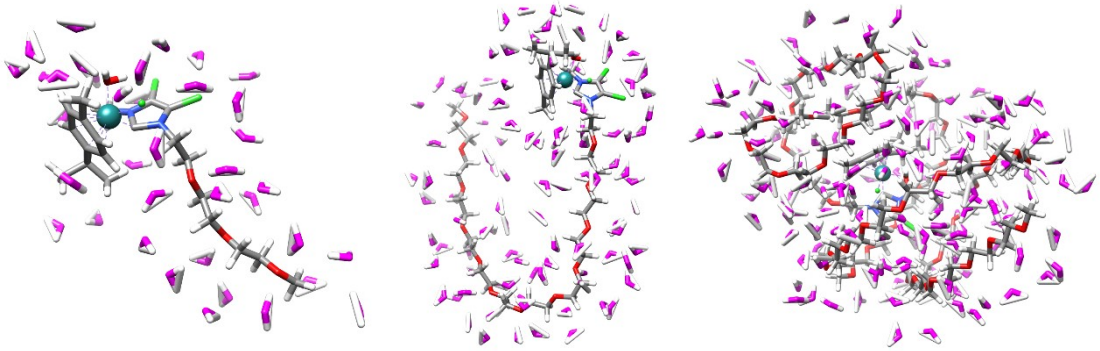

Figure S9. Molecular modelling of complexes **1-3** containing water molecules

S5.- CV data of complex 2 with different supporting electrolytes.

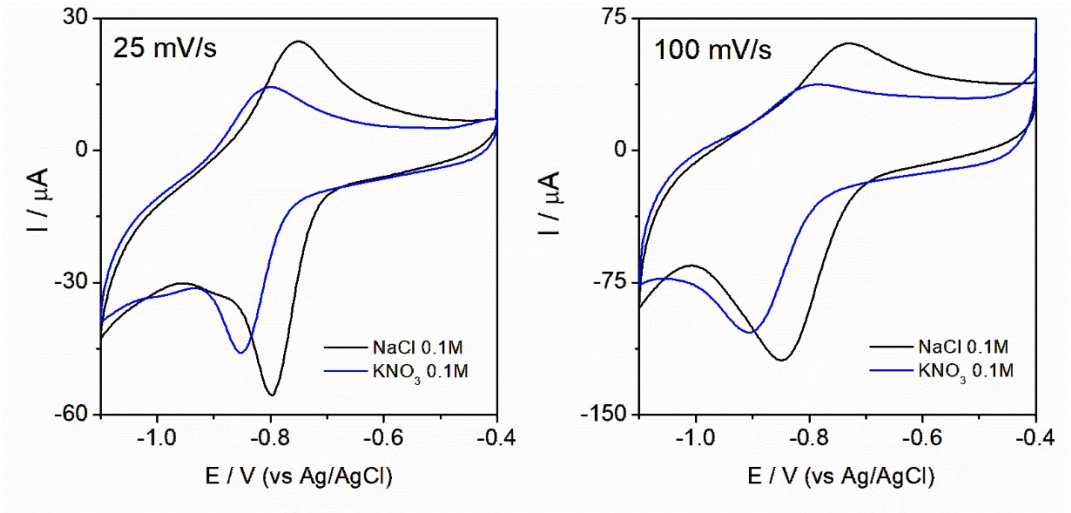

Figure S10. Cyclic voltammograms of complex **2** (potential range -1.1 to -0.4 V) in 0.1M NaCl (black) and 0.1 M KNO_3 (blue) at **(Left)** 25 mV/s and **(Right)** 100 mV/s.

S6.- Differences in ligands result in similar reduction potentials but different oxidation potentials for 1 and 2

Although complexes 1 and 2 exhibit nearly identical reduction potentials, their oxidation potentials differ significantly (Figure 4). This asymmetric redox could be explained if the ligands stabilise the reduced and oxidised states to different extents: if both ligands provide comparable stabilisation to the reduced Ru(I) form, E_{red} remain essentially unchanged. In contrast, variations in σ-donor/π-acceptor character, steric hindrance, and solvation effects can markedly alter the energy of the oxidised Ru(III) state, thus shifting the E_{ox} position.

Similar trends have been widely reported for coordination complexes where ligand modifications affect the HOMO and LUMO energies asymmetrically, leading to stronger perturbations in oxidation than in reduction processes. Theoretical and experimental analyses have demonstrated that oxidation potentials are generally more sensitive to ligand field strength, π-acceptor capacity, and reorganisation energy than reduction potentials. Eschwege and Conradie showed that reduction potentials correlate more directly with ligand LUMO energies, whereas oxidation potentials depend on broader electronic and geometric factors.[1] Da Silva further established a quantitative additivity model of ligand contributions to redox potentials, revealing that small substituent changes can induce significant shifts in E_{ox} without substantially affecting E_{red}.[2] In addition, recent studies on first-row transition-metal and Ru-based complexes have confirmed that peripheral ligand substitution can modify σ/π donation and molecular geometry, selectively influencing the oxidised state energy.[3,4]

Based on the above, 1 and 2 Ru-based complexes studied herein must comparable stabilisation of the reduced species (due to their similar E_{red}), whereas their different E_{ox} arise from gap ligand-induced modulation of the oxidised Ru(III) state through electronic, steric, and solvation effects.

References:

1.- Eschwege, K. G.; Conradie, J. *S. Afr. J. Chem.*, 2011, *64*, 203–21. *Redox Potentials of Ligands and Complexes – A DFT Approach.* https://scielo.org.za/pdf/sajc/v64/33.pdf

2.- da Silva, M. F. C. G. *Coord. Chem. Rev.*, 2012, *256*, 2907–2933. *Redox potential parameterization in coordination chemistry: The full additivity of ligand effects.* https://www.sciencedirect.com/science/article/abs/pii/S0013468612007050

3.- Boniolo, M.; et al. *Dalton Trans.*, 2021, *50*, 4467–4477. *Electronic and geometric structure effects on one-electron oxidation and reduction reactions in a series of first-row transition-metal complexes with the same pentapyridyl ligand framework.* https://pubs.rsc.org/en/content/articlehtml/2021/dt/d0dt03695a
4.- Busschaert, N.; et al. *Chem. Eur. J.*, 2021, *27*, 16583–16595. *Quantitative Assessment of Ligand Substituent Effects on σ- and π-Donor/Acceptor Properties in Metal Complexes.* https://onlinelibrary.wiley.com/doi/10.1002/chem.202104314

S7.- Stern-Volmer equation of complexes 1-3.

Table. S1. Stern-Volmer (K_{sv}) and biomolecular (k_q) quenching constants describing BSA-compounds interactions, calculated using fluorescence spectroscopy.

Complex	K_{SV} [M^{-1}]	R^2	k_q [M^{-1} s^{-1}]	logK_b
1	$(4.8 \pm 0.4) \times 10^3$	0.9951	$(9.8 \pm 0.7) \times 10^{11}$	3.7±0.5
2	$(1.1 \pm 0.09) \times 10^4$	0.9865	$(2.3 \pm 0.2) \times 10^{12}$	4.7±1.6
3	$(4.0 \pm 0.4) \times 10^3$	0.9649	$(8.0 \pm 0.9) \times 10^{11}$	2.5±0.5

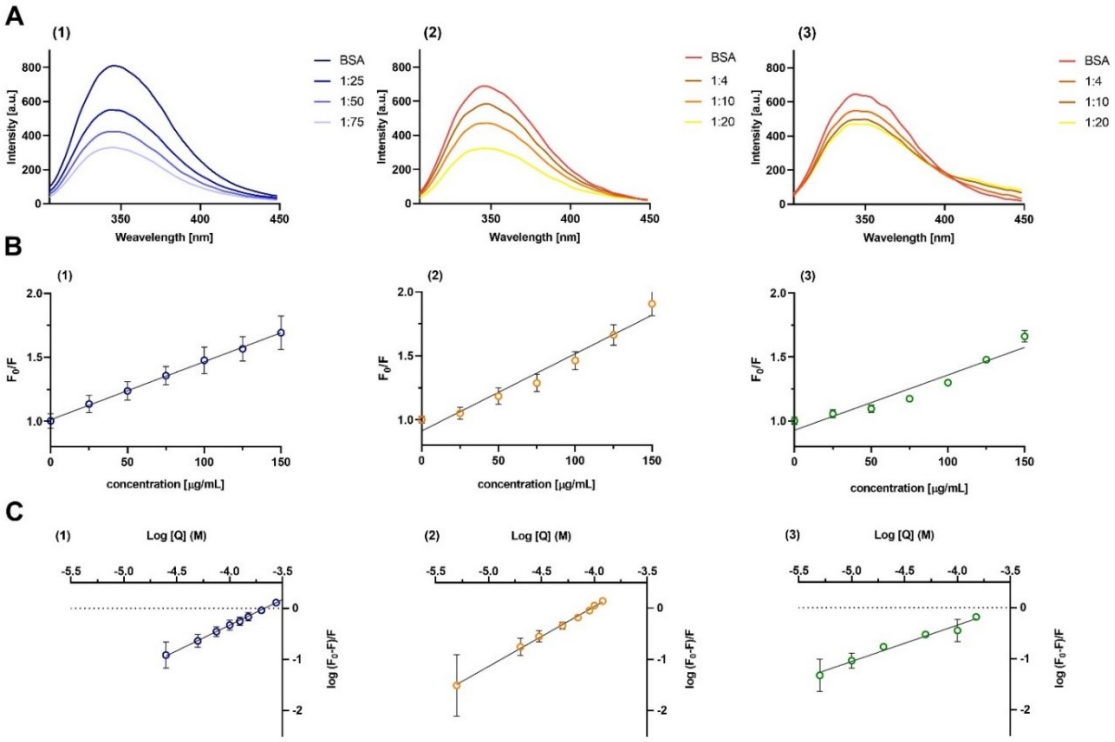

Figure S11. (A) Changes in tryptophan fluorescence intensity spectra after addition of complexes **1-3,** respectively. **(B)** Stern-Volmer plots, **(C)** double-logarithmic plots of fluorescence quenching. All measurements were conducted in phosphate buffer, 10 mmol/L, concentration of BSA, 5 µmol/L. Graphs represent mean ± SD, n = 3.

S8.- DLS, polydispersity and zeta potential data of complexes 1-3.

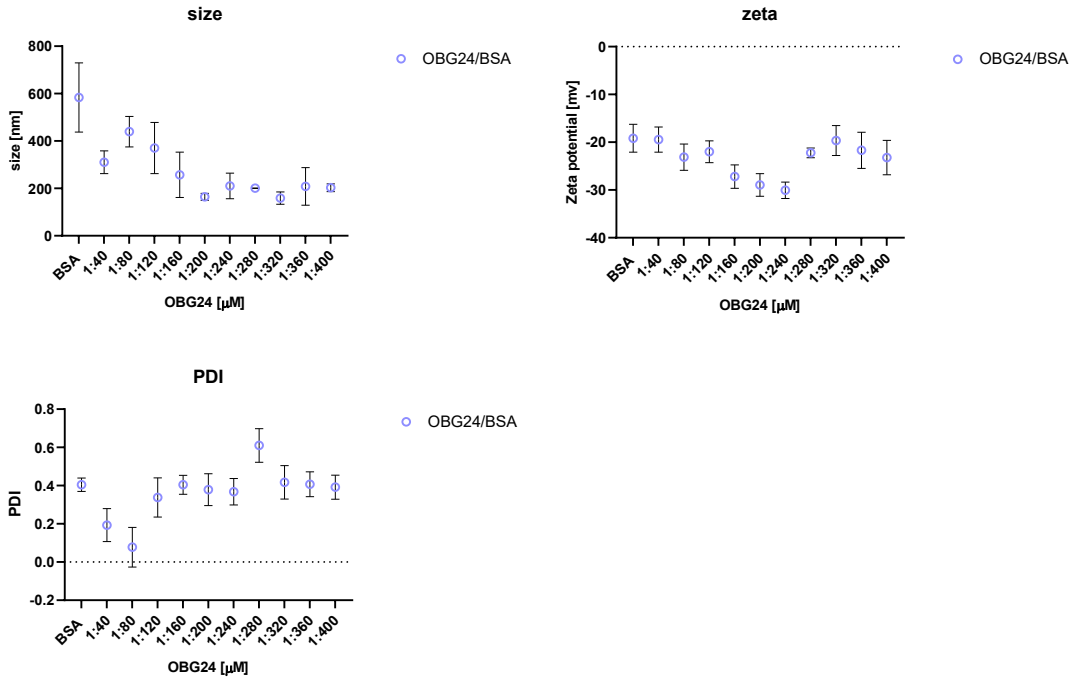

Figure S12. Graphs for hydrodynamic diameter (size and polydispersity) of BSA and changes in ζ-potential of BSA with increasing concentrations of complex **1**. Proteins concentration was 0.25 µmol/L (stock in phosphate buffer).

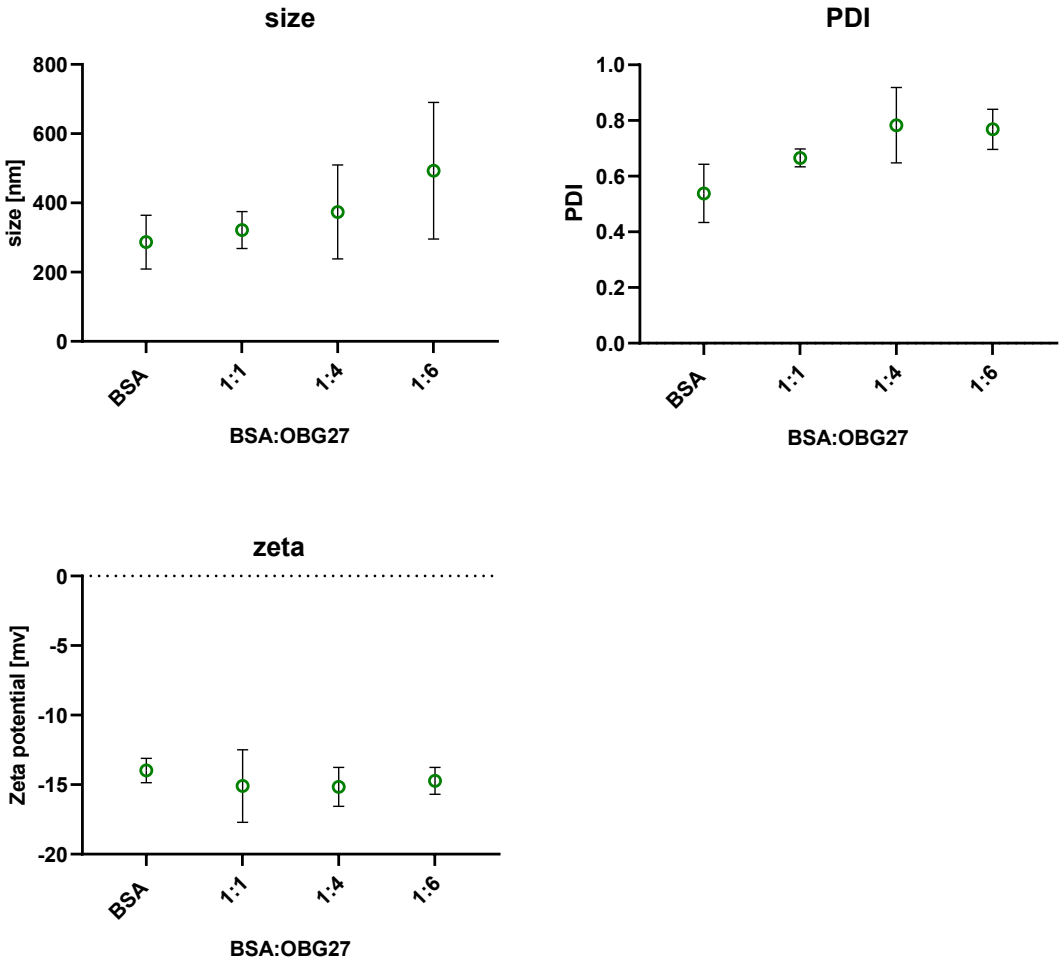

Figure S13. Graphs for hydrodynamic diameter (size and polydispersity) of BSA and changes in ζ-potential of BSA with increasing concentrations of complex **2**. Proteins concentration was 0.25 μmol/L (stock in phosphate buffer).

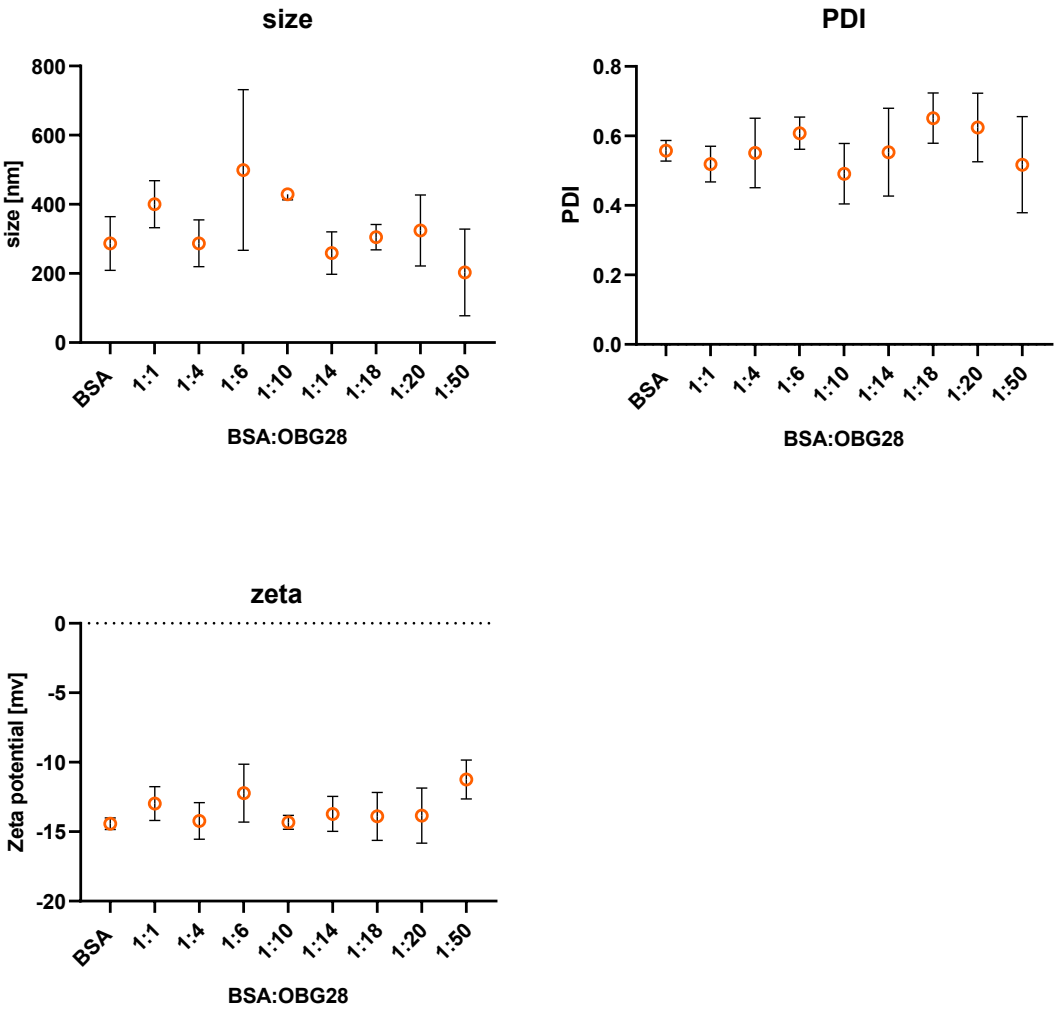

Figure S14. Graphs for hydrodynamic diameter (size and polydispersity) of BSA and changes in ζ-potential of BSA with increasing concentrations of complex **3**. Proteins concentration was 0.25 µmol/L (stock in phosphate buffer).

S9. Protocols of cell viability assay

The human hepatocellular carcinoma HepG2 cells line was purchased from the American Type Culture Collection (ATCC HB-8065, Rockville, MD, USA). The human hepatoma cell line Huh7 was purchased from Japanese Collection of Research Bioresources (JCRB 0403), Tsukuba, Ibaraki, Japan. The LNCaP, PC3, human prostate cancer cell lines, were procured from the American Type Culture Collection (ATCC CRL-1740, ATCC CRL-1435, respectively) (American Type Culture Collection, Rockville, MD, USA). All cell lines were genomically profiled before use.

Cell viability after treatment was analyzed by MTT assay. Therefore, prostate cancer cell lines PC3 and LNCaP as well as the human liver cancer cell lines HEpG2 and HuH7 cells were harvested (1.5 x 10^5 cells/well) into 12 well-plates. Same procedure was realized for the immortalized prostate cell line, PNT2 which serves as a healthy control cell line. After 48 hours and full adhesion of cells, they were treated with increasing doses of complexes **2** and **3** and their corresponding ligand precursor **L7** and **L8**, respectively. 0, 1, 3, 10, 30 and 100 mM doses of treatment. Short-PEG containing complex **1** was also tested on the immortalized PNT2 cell line so that to analyze its toxicity on healthy prostate cells and compared with longer-PEG containing compounds, such as complex **2** and **3**. After 24 hours of treatment, 100 μL of MTT 3-(4,5-dimethyl-2-thyazolyl)-2,5-2*H*-tetrazolium bromide) dye solution (Sigma-Aldrich) was added to each well and incubated at 37 ºC for 1 hour. Afterwards, medium was withdrawn and formed formazan crystals were dissolved with 2-propanol. Optical density of each well was measured by a microplate reader (iMARK, Bio-Rad Laboratories, Inc., Hercules, CA, USA) at 595 nm wavelength. Cell viability was expressed as the number of viable cells with respect to the vehicle-treated sample, which was assigned with 100% cell viability.

S10. Cell viability of complexes 2-3 and their corresponding precursor ligands, L7 and L8, in LNCaP and HuH7 cell lines.

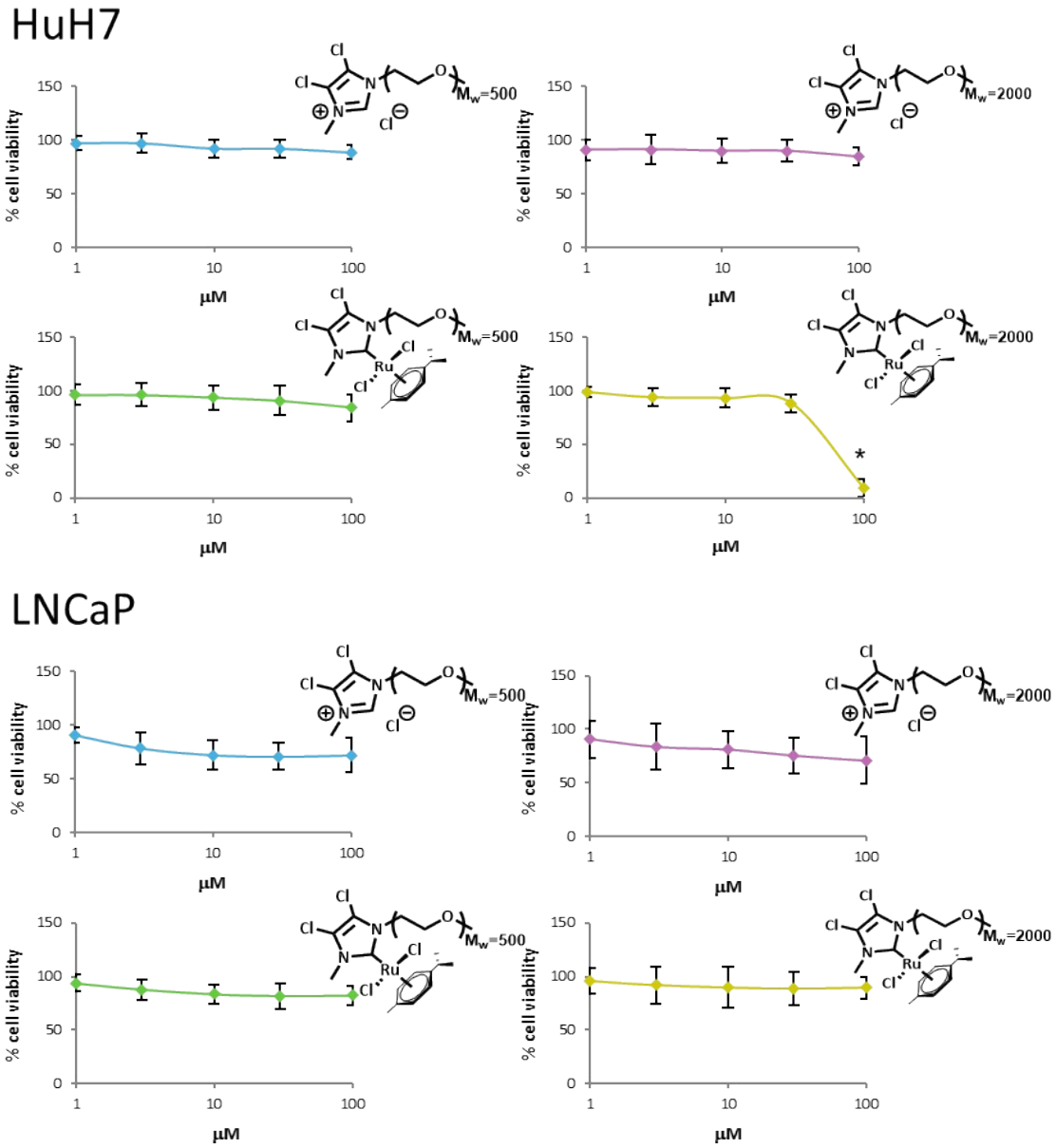

Figure S15. Cytotoxicity of complexes **2** and **3** and their corresponding ligand precursors, **L7** and **L8**. At the left, cell viability of the hepatic cancer cell line, HuH7, after treatment is represented. At the right, cell viability of the prostate cancer cell line, LNCaP, after treatment is represented. *, $p < 0.1$ significant differences between complex **2**-treated cells and the respective vehicle-treated cells by ANOVA test and Tukey test for multiple comparisons. Standards anticancer drugs in these cell lines cisplatin (3.9-93mM) or docetaxel (0.2mM-3.0mM) IC_{50} values recorded from literature (see section S12 in S.I.). Measurements were performed by three independent experiments, each performed in duplicate and using separately synthesized vials.

S11.- Cell viability of complexes 1-3 in PNT2 cell line, derived from normal human prostate epithelium cell lines.

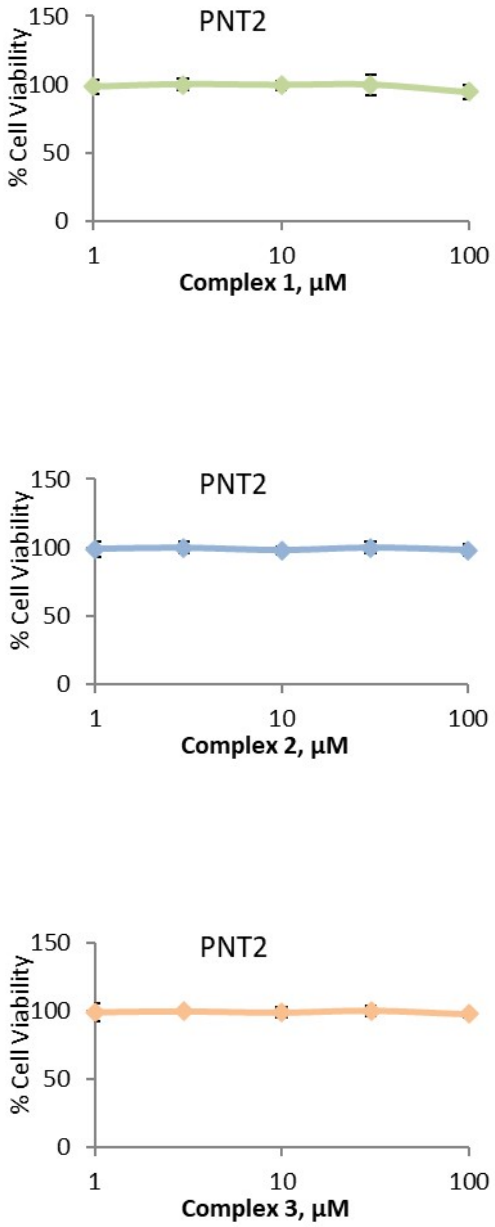

Figure S16. Cytotoxicity of complexes **1-3** by MTT on PNT2 cell line, derived from normal human prostate epithelium which is widely used as a non-tumorigenic control model. The study showed no toxicity up to 100 µM.

S12.- References for standard anticancer drugs

For instance, in 2024, Adamczuk et al. studied the cytotoxicity of cisplatin in three different cancer cell lines displaying distinct metabolic phenotypes. Cisplatin was observed to induce a dose-dependent reduction in the viability of LNCaP, PC-3, and DU-145 cancer cell lines. However, when testing cell viability across a dose range from 0 to 40 μM, IC_{50} values could only be determined for the LNCaP cell line (approximately 32 μM), as the effect on the other two cell lines was insufficient to fully reduce cell viability.[1] Nonetheless, PC-3 cell viability under cisplatin treatment was evaluated in 2019 by Masarik et al., together with a commonly used chemotherapeutic agent, docetaxel. Cisplatin-treated PC-3 cells exhibited IC_{50} values of 93 μM, whereas docetaxel appeared to be much more potent, reducing viability to 50% at a concentration of 201.3 nM.[2]

Furthermore, previous studies in our laboratory investigated the sensitivity of androgen-deprivation–sensitive (LNCaP) and androgen-deprivation–resistant (LNFLU) prostate cancer cell lines to docetaxel. In contrast to the trend observed for cisplatin, LNCaP cells appeared to withstand 10- and 20-μM docetaxel treatments, maintaining approximately 80% viability, whereas androgen-independent cell lines, as observed in PC-3, showed a markedly higher level of cell death, with around 60% of the population affected when using 10 μM and 20 μM doses. [3]

Regarding hepatocellular cancer cell lines, HepG2 and Huh7, during the recent study of Tsaroucha *et al.* about the effect of combining cisplatin treatment with the flavonoid apigenin, they could demonstrate the sensitization of both hepatocellular cell lines to cisplatin treatment. Overall, the data suggest a higher sensitization to cisplatin in HepG2. Therefore, when treating HepG2 and Huh7 cells during 48 h with cisplatin, 3.90 μM and 4.87 μM IC_{50} values where respectively found. [4] With respect to docetaxel effect on these two hepatocellular cancer cell lines, enhanced-docetaxel delivery was attended in advanced hepatocellular carcinoma (HCC). Herein, they found that free docetaxel exhibited low IC_{50} value on HepG2 cancer cell lines, around 3.0 μM (2.44 μg/ml). Docetaxel effect on Huh7 cancer cell line was not found in the literature. [5]

Hence, based on the results published in this field, both cisplatin and docetaxel exhibited much lower IC_{50} values than the Ru(II) complexes proposed here. The effects of these two well-known anticancer agents on prostate and hepatocellular cancer cell lines consistently remained below 100 μM. In the case of cisplatin, the highest IC_{50} value was observed in PC-3 cancer cell lines, where, interestingly, the highest value for docetaxel

treatment was also found. Although some effect was observed for compound **3** in hepatocellular cancer cell lines, those values are by no means comparable to those exhibited by cisplatin in both HepG2 and Huh7 cell lines, which were found to be in the range of 3 to 5 μM.

References:

1.- G. Adamczuk, E. Humeniuk, K. Adamczuk, A. Grabarska, B. Madej-Czerwonka, M. Michalczuk, A. Korga-Plewko and J. Dudka, *Ann. Agric. Environ. Med.,* **2024**, *31*, 37–46.

2.- M. Raudenska, M. Kratochvilova, T. Vicar, J. Gumulec, J. Balvan, H. Polanska, J. Pribyl and M. Masarik, *Scientific Reports,* **2019**, *9*, 1660.

3.- O. Barrios, B. G. Sánchez, T. Rodríguez-Prieto, J. Cano, A. Bort, R. Gómez and I. Díaz-Laviada, *Biomacromolecules,* **2022**, *23*, 5043–5055.

4.- F. Papachristou, N. Anninou, G. Koukoulis, S. Paraskakis, E. Sertaridou, C. Tsalikidis, M. Pitiakoudis, C. Simopoulos and A. Tsaroucha, *Mutation Research/Genetic Toxicology and Environmental Mutagenesis,* **2021**, *866*, 503352.

5.- Y. Yao, Y. Hu, X. Meng, F. Feng, F. Xu, G. Wang, H. Yu and J. Li, *Pharmaceutical Science Advances,* 2024, **2**, 100046.

S13.- Protocols for transfer hydrogenation reactions.

Catalytic cyclohexanone reduction

In 1 ml of deuterated water, the ruthenium catalyst complex **1**, **2** or **3** ($3.3 \cdot 10^{-3}$ mmol), NaCOOH (0.17 mmol, 11.3 mg) and cyclohexanone (0.03 mmol, 3.3 μL) were dissolved, obtaining a molar ratio of 1:10:50 (catalyst:cyclohexanone:NaCOOH). Afterwards, 0.5 mL of the solution was transferred into an NMR valved tube and heated in an oil bath at 80 ºC. The experiments were monitored by NMR prior to heating and after heating for 0.5, 1, 2, 4, 6 and 24 hours.

Catalytic NAD^+ reduction

The same protocol as described above was repeated using NAD^+ (0.03 mmol, 21.99 mg) as substrate. The reaction was conducted at room temperature.

Catalytic NAD^+ reduction with 2-BSA

The procedure was repeated with NAD^+ (0.03 mmol, 21.99 mg), using complex **2** pre-incubated with BSA (54.62 mg, 8.28×10^{-4} mmol) at a 4:1 molar ratio (2:BSA) in 1 mL of D_2O for 10 minutes. Subsequently, NAD^+ and NaCOOH were added to the solution for the catalytic study at room temperature.

Catalytic NAD^+ reduction with 2-micelles

Micelles were synthesised following the protocol established by the research group, using cationic and anionic cholesterol dendrons ($ChG_2(NM_3^+)_4$ and $ChG_2(SO_3^-)_4$). Briefly, 3.3 mg of complex **2** (30 % w/w) and 11.3 mg of dendron were dissolved in 0.5 mL of deuterated water and stirred overnight. Subsequently, 9.5 mL of 20 mM NaCl in D_2O were added and stirred for 5 minutes. Then, NaCOOH (0.17 mmol, 11.3 mg) and cyclohexanone (0.03 mmol, 3.3 µL) were included into the solution. Later, 0.5 mL of the solution was transferred into a NMR tube, and its evolution was tracked at the following time intervals using NMR spectroscopy at room temperature: 0, 0.5, 1, 2, 4, 6, and 24 hours.

Determination of the TON and TOF Values.

Catalytic activity was evaluated using 3-(trimethylsilyl)-2,2,3,3-tetradeuteropropionic acid (TMSP-d_4) as an internal reference, allowing the change in substrate integrals to be tracked over time. In the ^{1}H-NMR (D_2O) spectra, the signals at 2.23 ppm (m, 4H, CH_2CH_2CO) for cyclohexanone and 9.20 ppm (s, 1H, $NCHCCONH_2$) for NAD^+ were employed to calculate TON and TOF. The integral at the starting time was considered as 100 % of substrate and subsequent values were determined using the following formula:

$$TON = \frac{It}{Io}\frac{[substrate]}{[catalyst]} \qquad TOF = \frac{TON}{hours}$$

Where, I_0 represents the integral of the substrate at the initial time, and I_t corresponds to the product at given time point. I_t was calculated by subtracting the integral of the substrate specific time (e.g., 6 or 24 hours) from its initial integral, I_0.

S14.- Reaction profiles of compound 4 in TH.

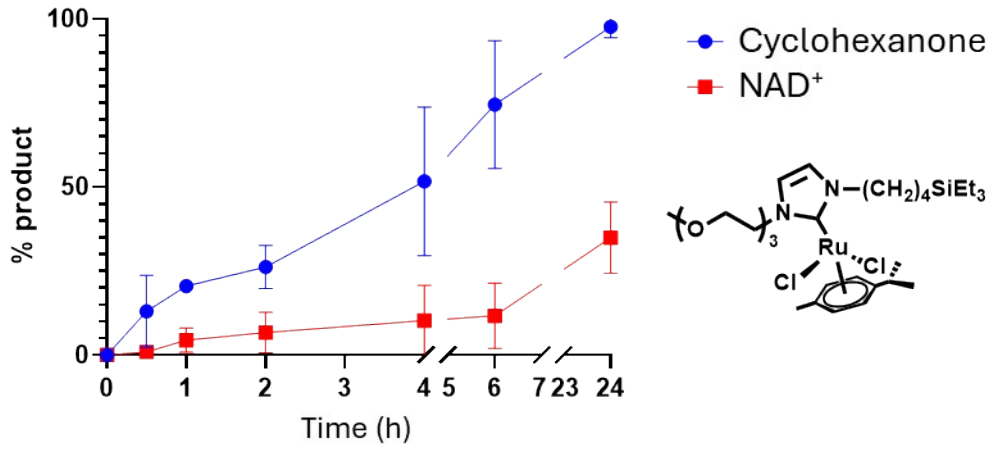

Figure S17: Reaction profile of complex [$RuCl_2$(η^6-p-cymene)(triethylsilylbutyl-NHC-PEG_{147})] using cyclohexanone or NAD^+ as substrates.